Temperature dependencies of the relaxation, order and segregation at a $\Sigma = 5$ (210) [001] tilt grain boundary in Cu_3Au

1996 J. Phys.: Condens. Matter 8 6833

(http://iopscience.iop.org/0953-8984/8/37/006)

J. Phys.: Condens. Matter **8** (1996) 6833–6849. Printed in the UK

Temperature dependencies of the relaxation, order and segregation at a $\Sigma = 5$ (210) [001] tilt grain boundary in Cu_3Au

M El Azzaoui and M Hou

Physique des Solides Irradiés CP234, Université Libre de Bruxelles, Boulevard du Triomphe, B-1050 Brussels, Belgium

Received 7 March 1996, in final form 15 May 1996

Abstract. The thermal dependence of the relaxation, order and segregation in the vicinity of a $\Sigma = 5$ (210) [001] tilt grain boundary in the Cu_3Au $L1_2$ binary alloy is investigated by means of computer simulation with an empirical N-body potential. Energy minimization is performed in order to estimate the particularly strong relaxation effects in the vicinity of the boundary plane at 0 K. Monte Carlo simulations are carried out for constant chemical potential, number of particles, volume and temperature in order to study the thermal properties of the system. Detail is provided plane by plane, parallel to the boundary, which characterizes the temperature dependencies of the order, segregation, sublattice occupancy and relaxation. The vicinity of the boundary remains strongly affected by atomic relaxation and segregation at all temperatures, although no simple relation between relaxation and segregation is found. The evolution of long-range order and sublattice occupancy are strikingly different in the close vicinity of the boundary plane to those in the bulk. The boundary plane is fully disordered at all temperatures between $0.2\,T_c$ and $1.5\,T_c$, where T_c is the bulk temperature for the order–disorder phase transition. The transition to bulk properties with distance from the boundary is characterized quantitatively.

The influence of the potential model is emphasized by means of a comparison between the results obtained with two somewhat different N-body potentials of similar nature.

1. Introduction

$L1_2$ intermetallic compounds are receiving considerable attention because of their particular physical properties and possible technological applications. On the one hand, their mechanical properties are the subject of several studies [1] and on the other, their thermodynamic properties display many interesting features like solid phase transitions, which had already been noticed eighty years ago [2], wetting at antiphase boundaries [3, 4], and segregation [5].

These macroscopic features are driven by the material properties at the microscopic and even the atomic scale. The order–disorder solid phase transition is known to nucleate at interfaces and to wet them. It may also be expected to nucleate at point defects or point defect clusters. Segregation depends on the interatomic arrangement at interfaces where interplanar and atomic relaxation occurs.

Cu_3Au is the only $L1_2$ alloy which does not fracture at grain boundaries. Therefore, stress is expected to promote no major mechanical modification, for a wide range of conditions under which the study of continuous thermodynamic evolution is thus possible. In addition, Cu_3Au has an order–disorder transition temperature of 663 K, well below the

0953-8984/96/376833+17$19.50

melting point, and this allows one to investigate the influence of such a solid phase change on interface properties. Since both the performances of experiments and theoretical tools for studies at the atomic scale are currently developing quickly, a feedback between atomistic modelling and direct observation methods has become realistic.

A major breakthrough in atomistic modelling occurred with the introduction of the tight-binding approximation [6, 7] and, later, of the embedded-atom model [8] as a basis on which to study the cohesion of metals and metallic alloys. The non-additive potentials which are empirically derived from these models have been widely assessed with the aim of providing reasonable descriptions of the metal properties. Since they also turn out to be almost as efficient as pair potentials in computer modelling, they allow one to perform large-scale molecular dynamics (MD) and Monte Carlo (MC) simulations within affordable computer times, even on workstations.

Molecular dynamics provides a full description of particle trajectories in time and allows time averages to be calculated which makes it possible to establish the relationship between microscopic and macroscopic aspects of the evolution of a system. Characteristic times for thermodynamic evolution may however be very long (segregation for instance is well known to extend up to the 100-hours range). Therefore, the Monte Carlo technique for sampling configurations in phase space may be an advantageous alternative. Thus, for the sake of efficiency, the two methodologies may be combined and adapted to particular atomic-scale problems.

Interface relaxation has been predicted for a wide variety of systems by using a damping technique in MD for energy minimization at 0 K. There are fewer estimates of relaxation at high temperature although, as will be shown in the present work, it may be an important issue. Such estimates can be performed either by the MD or the MC methods. The order–disorder phase transition has been approached by several different methods. The Ising model allows one predict this transition as the result of particle exchanges on fixed atomic sites [4]. This technique has some resemblance to the Monte Carlo method applied to a rigid lattice and sampling phase space by means of particle exchange [9]. A variant of this method allows lattice expansion in order to maintain constant pressure [10]. A more general scheme applies to an ensemble close to the grand canonical one, in which the chemical potential as well as the number of particles are kept constant [11] and which also accounts for individual atomic relaxations. This ensemble has been termed the *transmutational* ensemble [12] and was successfully applied to MC modelling of segregation in dilute binary alloy solutions [12–14].

$L1_2$ structures have already been the subject of many studies, motivated by, among other factors, the relationship between the strength of segregation and the mechanical properties of these compounds [15]. In [15], the authors compare the composition in a wide variety of grain boundaries in Cu_3Au and Ni_3Al at room temperature and somewhat below the temperature for the bulk order–disorder transition in Cu_3Au.

In the present work, a similar transmutational MC method is used to quantitatively study the thermal evolution of a Cu_3Au bicrystal in the vicinity of a high-angle grain boundary, $\Sigma = 5$ (210) [001], in combination with MD with damping for relaxation studies. The interest of the $\Sigma = 5$ (210) [001] tilt boundary in Cu_3Au lies in the fact that its thermal evolution involves both exceptionally strong relaxation and segregation. Therefore, independently of its interest in materials science, it represents a case study which is ideally suited for looking at the possible interplay between relaxation, order and segregation in detail. To what extent these properties, specific to this interface, are related to the order state in the neighbouring matrix is also investigated in detail.

The computational methodologies used are briefly described in the next section. Section

3 then provides an atomic-scale description of the dependence of the interplay between segregation, relaxation and order on temperature in the vicinity of the boundary. The influence of the model used on the results is discussed in section 4.

2. The model and computation

2.1. Potentials

The basic parameter which governs MD and MC simulations in condensed matter is the potential. Many variants of empirical N-body potentials have been suggested. Usually, they are fitted to bulk material properties extrapolated to 0 K, and applied at high temperatures. The extent to which this procedure is reasonable, and whether it also applies to inhomogeneities like interfaces, is only *a priori* speculative. Therefore, it is useful to compare the results obtained with somewhat different potentials in order to estimate the sensitivity of the simulation results to the model. Non-sensitive features may then be considered as reasonable predictions, while the sensitive ones may be useful for refining the empirical model used on the basis of experimental evidence.

Two model potentials are considered here, both making use of the same functional dependence as the second-moment tight-binding approximation.

2.1.1. Model potential A. The first model used in our simulation was developed by Ackland and Vitek [16]. It is described in terms of the empirical N-body potential suggested by Finnis and Sinclair [7].

The total energy of a system is given by

$$E = \sum_{\substack{i=1 \\ j\neq i}}^{N} V(r_{ij}) - \left[\sum_{\substack{i=1 \\ j\neq i}}^{N} \phi(r_{ij}) \right]^{1/2} \tag{1}$$

where r_{ij} is the separation between atom i and its neighbour j. $V(r)$ is associated with repulsion between the core electrons at sites i and j. The square root models d-band bonding. $\phi(r)$ represents the sum of the squares of the overlap integrals.

V and ϕ are fitted to the experimental values of the lattice constant, cohesive energy, elastic constants, vacancy formation energy and stacking fault energy. For the binary alloy they are denoted as $V_{\alpha\alpha}, V_{\alpha\beta}, V_{\beta\beta}, \phi_{\alpha\alpha}, \phi_{\alpha\beta}, \phi_{\beta\beta}$. The subscripts α and β refer to the atomic species α and β. The functions $V_{\alpha\alpha}, V_{\beta\beta}, \phi_{\alpha\alpha}, \phi_{\beta\beta}$ are identical to those for pure metals [17]. $\phi_{\alpha\beta}$ was taken as the geometrical mean of $\phi_{\alpha\alpha}$ and $\phi_{\beta\beta}$.

Only $V_{\alpha\beta}$ is fitted to the alloy properties, and the functions which make up this present model consist of cubic splines [16]:

$$V_{\alpha\beta}(r_{ij}) = \sum_{k=1}^{6} a_k^{\alpha\beta} H(r_k^{\alpha\beta} - r_{ij})(r_k^{\alpha\beta} - r_{ij})^3 \tag{2}$$

$$\phi_{\alpha\alpha}(r_{ij}) = \sum_{k=1}^{2} A_k^{\alpha\alpha} H(R_k^{\alpha\alpha} - r_{ij})(R_k^{\alpha\alpha} - r_{ij})^3 \tag{3}$$

and

$$\phi_{\alpha\beta}(r_{ij}) = \sqrt{\phi_{\alpha\alpha}(r_{ij})\phi_{\beta\beta}(r_{ij})} \tag{4}$$

where $H(x)$ is the Heaviside step function which gives the cut-off distance of each spline segment. The model potential A parameters are given in [16].

The range of this potential is limited to between the third- and the fourth-neighbour distances.

2.1.2. Model potential B. This model potential is based on the scheme suggested in [6].

The total energy of the alloy is given by [9, 18]:

$$E = \sum_{\alpha}\sum_{i}^{N_\alpha}\left\{\sum_{\beta}\sum_{\substack{j=1\\ i\neq j}}^{N_\beta} A_{\alpha\beta}\exp\left[-p_{\alpha\beta}\left(\frac{r_{ij}}{d_{\alpha\beta}}-1\right)\right] - \left[\sum_{\beta}\sum_{\substack{j=1\\ i\neq j}}^{N_\beta}\xi_{\alpha\beta}^2\exp\left[-2q_{\alpha\beta}\left(\frac{r_{ij}}{d_{\alpha\beta}}-1\right)\right]\right]^{1/2}\right\} \tag{5}$$

where r_{ij} is the distance between particles at sites j and i. α (β) refers to the two different kinds of atom and i (j) runs over all particles of type α (β). The parameters $p_{\alpha\beta}$, $q_{\alpha\beta}$, $A_{\alpha\beta}$, and $\xi_{\alpha\beta}$ are fitted to the experimental values of the cohesive energy, the equilibrium equation, and the elastic constants of the pure Cu and Au elements and the compound Cu_3Au [9]. The range of this potential is limited to between the fifth- and the sixth-neighbour distances and is thus somewhat larger than that of the model potential A. The model potential B parameters are given in [9].

2.2. Geometrical models

A number of configurations of the boundary between two grains can be predicted for the same coincidence-site lattice, each one corresponding to a different rigid-body translation of one grain with respect to the other. The boundary planes have either pure copper or mixed Cu–Au composition [19, 20].

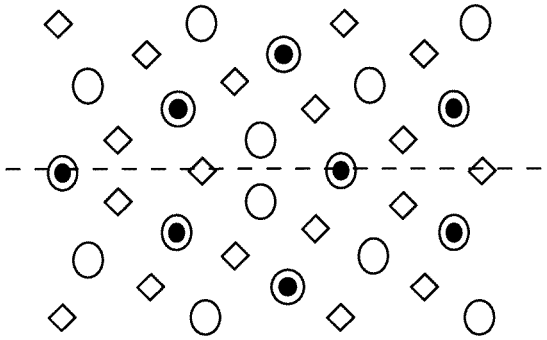

Figure 1. The symmetrical geometrical configuration S_{51} of the $\Sigma = 5$ (210) [001] tilt boundary in Cu_3Au. Open circles and diamonds represent copper atoms at $z = 0$ and $z = \pm 0.5$ respectively, and black circles represent gold atoms at $z = 0$. The dashed line is drawn to show the position of the boundary plane. Other variants with higher excess energies are given in [21].

Among the possible variants, we selected that observed by HREM and denoted as S_{51} in [21]. As shown in figure 1, the boundary plane is of mixed composition.

For the simulations, a box of atoms is constructed with edges X, Y and Z along the [001], [$\bar{1}$20] and [210] crystallographic directions respectively. The box size was 4[001] $\times$ 3[120] $\times$ 6[210] lattice cells, which represents 1440 particles (360 gold atoms and 1080 copper atoms). The (210) boundary is placed for convenience at the centre of the box. Periodic boundary conditions are applied in the X-, Y- and Z-directions in order to mimic an infinite crystal. This procedure generates periodic images of the boundary plane. Care is taken to make the box size large enough to avoid interactions between the boundary plane and its images. Such an interaction is considered negligible when an area is preserved between the boundary plane and its image with both static and dynamic bulk properties.

2.3. Energy minimization

The geometrical box described above was relaxed by means of MD with damping forces according to the procedure first suggested by Bennet [22]. This algorithm is easily implemented in molecular dynamics programs and allows for the energy minimization and tests of the stability at 0 K. We consider that the minimization procedure is achieved when the potential energy of the system does not change by more than $\delta U/U \approx 10^{-6}$ over a set of 3000 damping time-steps of 2 ps. The periodic boundary conditions allow the system to freely undergo a rigid-body translation during the minimization, provided that an energy minimum associated with such a translation is close enough to the initial configuration.

Introducing a grain boundary into a small geometrically uniform system results in a non-zero stress tensor because of both the interfacial tension and finite-size effects. The former is real and should be preserved in the simulations. The box size is adjusted in such a way that the stress component σ_{zz} normal to the boundary plane vanishes and the tangential components, σ_{xx} and σ_{yy}, which reflect the contribution of the interfacial tension, remain non-zero.

The magnitude of the relaxation at the plane n is defined by the coefficient

$$\left(\frac{\Delta d}{d}\right)_{(420)} = \frac{z_n(T) - z_{n-1}(T)}{d_{(420)}(T)} - 1 \tag{6}$$

where $z_n(T) - z_{n-1}(T)$ is the distance between planes n and $n-1$ and $d_{(420)}(T)$ is the separation between neighbour planes of the {420} family at temperature T. With this definition, a positive value of $(\Delta d/d)_{(420)}$ reflects an expansion while a negative value reflects a contraction.

2.4. The Monte Carlo simulation technique

The Metropolis Monte Carlo method employed here is based on the original work by Foiles [11]. A modified grand canonical ensemble is used, in which total number of atoms, temperature, volume and chemical potential difference $\Delta\mu = \mu_{Au} - \mu_{Cu}$, corresponding to the bulk composition, are fixed. The simulations are carried out in three steps.

In a first step, an atom selected at random is displaced from its current position by a random vector. The magnitude of this vector is dynamically adjusted in order to monitor the rate of acceptance. The decision to accept this new configuration is based on the relative probability

$$\frac{P_{new}}{P_{old}} = \exp(-\beta\,\Delta U). \tag{7}$$

The trial is repeated for all atoms in the simulation box. This step allows for relaxation at the atomic scale induced by either thermal vibrations or local structural changes. It also

allows for rigid-body translations as the result of a series of accepted individual moves.

In the second step, the chemical identity of the atom selected in the first step is changed. The decision to accept this new configuration is based on the relative probability

$$\frac{P_{new}}{P_{old}} = \exp[-\beta(\Delta U \pm \Delta\mu)]. \tag{8}$$

This transmutation trial allows for local compositional change and segregation.

A third step allows for a site exchange of this atom with any other selected at random in the simulation box. The decision to accept this new configuration is based on the relative probability given in equation (7). This trial, equivalent to that used in Ising procedures, also contributes to local composition and order changes in the alloy. In practice, the rate of acceptance in this third step is found to be much smaller than that in the second step.

Modification of both local order and composition induces changes in the surface tension at the boundary. Therefore, variations in the surface tension are allowed in the present simulations. This is why the simulations are performed for constant volume rather than for constant pressure. The simulation box is chosen large enough to ensure that whatever change occurs at the grain boundary, both the mechanical and the thermodynamic properties of the bulk area remain identical to those of a perfect crystal.

The relative probability in equation (8) implies that the dependence of $\Delta\mu$ on composition needs to be known prior to the grain boundary simulations being performed. In order to establish the relationship between $\Delta\mu$ and the temperature, MC simulations with a Cu_3Au single crystal are performed. A box of 500 atoms was found to be sufficiently large therefore. Results are given in figure 2 for three different temperatures.

2.5. The order parameter

The state of order of the system is determined by computing average values of an appropriate long-range-order parameter (LRO), $\eta(z, T)$, on a layer-by-layer basis. The order was determined for each (210) mixed atomic plane parallel to the boundary inside the simulation box. At low temperature, the ordered structure of the alloy is made up of four simple cubic sublattices: three are occupied by Cu atoms (α-sites) and the fourth by Au atoms (β-sites). The LRO parameter can be defined plane by plane, parallel to the boundary plane according to the following relation:

$$\eta(z, T) = p^{\beta}_{\mathrm{Au}}(z, T) - p^{\alpha}_{\mathrm{Au}}(z, T) \tag{9a}$$

or

$$\eta(z, T) = p^{\beta}_{\mathrm{Au}}(z, T) - (1 - p^{\alpha}_{\mathrm{Cu}}(z, T)) \tag{9b}$$

where z is the coordinate of the plane. $p^{\beta}_{\mathrm{Au}}(z, T)$ and $p^{\alpha}_{\mathrm{Cu}}(z, T)$ respectively denote the fraction of gold sites in the plane at z occupied by gold atoms and that of copper sites occupied by copper atoms.

If no segregation occurs in the Cu–Au plane at z, $\eta(z, T)$ is unity in the ordered state and is zero for the disordered one. It is identically zero for pure Cu layers. This order parameter is identical to that used in the mean-field theory as applied to the study of alloy surfaces [23].

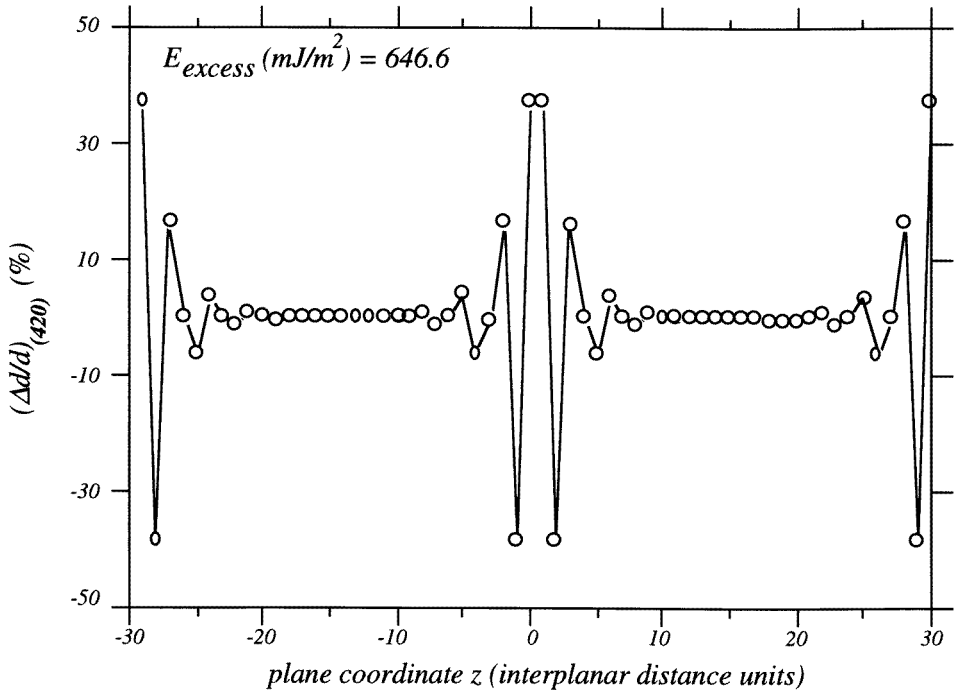

Figure 2. The isothermal dependence of the chemical potential on the concentration of gold. These results are obtained with the model potential A.

3. Results

3.1. The configuration of the $\Sigma = 5$ (210) [001] *tilt boundary at 0 K*

Combined high-resolution electron microscopy, computer modelling, and image simulations were used to study the structure of the $\Sigma = 5$ (210) [001] tilt boundary in the ordered compound Cu_3Au, and the results obtained by energy minimization are discussed in [21].

Among all possible variants, the configuration S_{51} shown in figure 1 has the lowest excess energy.

The interplanar spacing $(\Delta d/d)_{(210)}$ for Cu–Au planes close to the boundary plane was determined from the HREM simulated image [21]. A good agreement is found with the present energy-minimization results. This agreement is confirmed with the model A potential.

Model A was selected in the present work in order to investigate the thermal behaviour of the $\Sigma = 5$ (210) [001] tilt boundary in ordered Cu_3Au. The associated critical temperature found with this potential is $T_c = 590 \pm 20$ K, which is only 10% lower than the experimental value. The results will then be compared with those obtained with model B.

Figure 3 displays the relaxation profile normal to the boundary plane. The excess S_{51} interfacial energy after energy minimization is given in the inset.

Although no experimental measure for this interfacial excess energy is available, the order of magnitude is consistent with simulation results found in the literature for one-component solids [17] and for alloys [24].

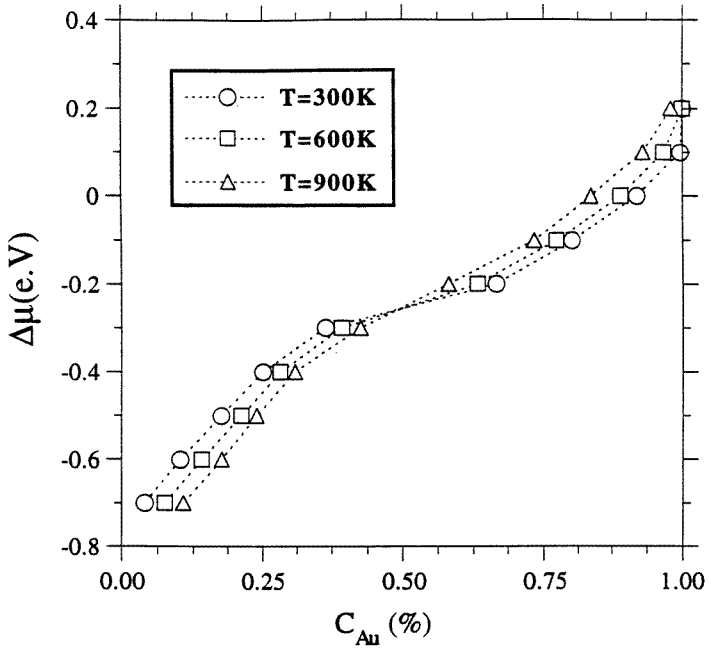

Figure 3. The interplanar relaxation profile. The central boundary plane is at $z = 0$, and its image generated by the periodic boundary conditions is at $z = 30$. The excess internal energy of the grain boundary is given as an inset.

Table 1. Characteristics of the S_{51} boundary after minimization. σ_{xx} and σ_{yy} are the contributions of the boundary interface, and σ_{zz} was measured in the bulk area. These two latter components vanish in the bulk. The results obtained with the model potentials A and B are given at 0 K.

	σ_{xx} (kbar)	σ_{yy} (kbar)	σ_{zz} (kbar)	$\Delta L/L$	E_{excess} (mJ m^{-2})
Model A, 0 K	5.26	5.14	0.0	0.0102	646.6
Model B, 0 K	5.12	4.93	0.0	0.0150	687.3

The expansion at the boundary of about 40% is followed by a contraction of the same magnitude. Such a strong relaxation substantially affects the stress component along the direction normal to the interface. This component is reduced to zero by means of the minimization procedure described in section 2.3. Table 1 gives the equilibrium stress components, the expansion coefficient normal to the grain boundary plane, denoted $\Delta L/L$, and the excess energy.

3.2. MC simulations

3.2.1. The order–disorder transition. In what follows, the temperatures are scaled to T_c for convenience, according to the procedure used in [25]. For each simulation, a first series of two hundred thousand Monte Carlo steps (including each of the three elementary steps described by equations (7) and (8)) is necessary to reach equilibrium. Eight hundred thousand further steps are used to compute mean quantities. In this way, it is ensured that

typical statistical uncertainties are never more than 10%.

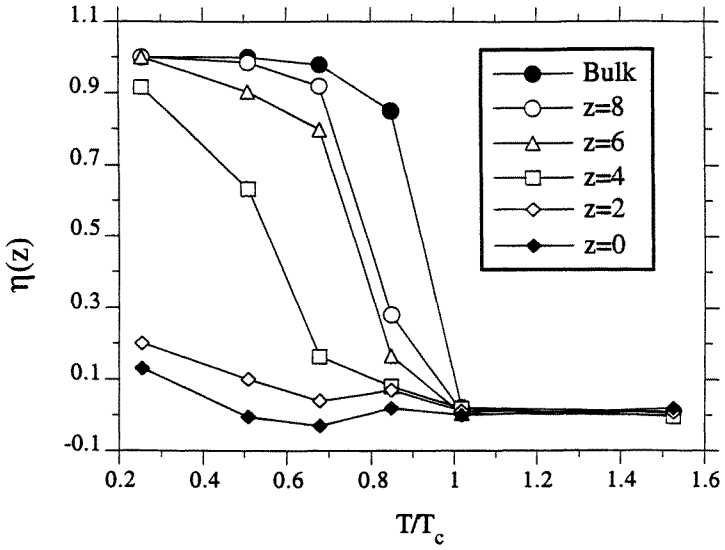

Figure 4. The order parameter as a function of temperature for different atomic planes and for the bulk. $z = 0$ corresponds to the position of the grain boundary plane. The results are only provided for the initially mixed planes.

Figure 4 represents the thermal dependence of the order parameter η defined plane by plane by equation (9) in the vicinity of the grain boundary as well as in the bulk of perfect Cu_3Au single crystal. Ten planes away from the grain boundary—that is, at a distance smaller than 1 nm—the thermal dependence of η can no longer be distinguished from that in the bulk perfect crystal. In the bulk region, η displays a sharp drop at around T_c characteristic of a first-order phase transition. The closer the plane is to the boundary plane, the smoother the drop is. In the boundary itself and its first-neighbour mixed plane ($z = 2$), the thermal evolution of η is insignificant with respect to the limit of accuracy of our simulations and it is characterized by values close to zero at all of the temperatures investigated, even well below the transition temperature T_c. The influence of the bulk already shows up in the next mixed plane at $z = 4$.

Several factors may be considered as contributing to the difference between the boundary and the bulk temperature dependencies of the order parameter. These factors are studied in the following sections. Since η combines $p^{\beta}_{\mathrm{Au}}(z, T)$ and $p^{\alpha}_{\mathrm{Cu}}(z, T)$, it does not allow an explicit characterization of segregation, which is now considered.

3.2.2. Segregation effects. Figure 5 shows the temperature dependence of the gold concentration in the mixed planes around the grain boundary. The results are compared with those in a perfect crystal.

This concentration is 0.5 in a perfectly ordered lattice and it is 0.25 in a fully disordered one. Again the case of the boundary plane is quite different from the bulk case. This difference affects a zone around the boundary which is limited to 1 nm. At low temperature, a strong segregation is found in the boundary and its next-neighbour mixed planes, where the order parameter remains close to zero at all temperatures. At $0.25\,T_c$, these planes are 90%

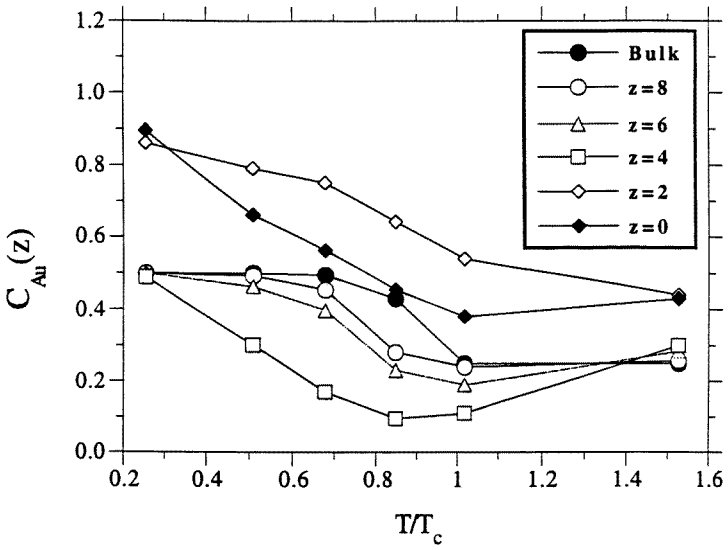

Figure 5. The gold concentration represented plane by plane as a function of temperature. Only the initially mixed planes are considered. The thermal dependence of the mixed-plane gold concentration in the bulk is shown for comparison. The grain boundary plane is at $z = 0$.

gold. This contrasts with the case of the $\Sigma = 5$ (100) (reference [25]) and the $\Sigma = 3$ (111) (reference [26]) boundaries for which neither significant segregation nor relaxation is found.

Such a strong segregation smoothly decreases with increasing temperature and displays no sharp variation around T_c. The segregation persists in the boundary plane and its next-nearest-neighbour mixed planes at high temperature, way above T_c. This contrasts with the situation in the second-nearest-neighbour mixed planes ($z = 4$) where the gold concentration presents a minimum close to T_c, well below the value of 0.25 characteristic of disorder in the bulk. This indicates the temperature-dependent segregation of copper. The copper segregation persists in the plane at $z = 6$ and disappears at $z = 8$, where the thermal dependence of the gold concentration is the same as that further into the bulk.

Like that of the order parameter, the thermal dependencies of the gold and copper concentrations are thus quite different in the close vicinity of the boundary plane to that in the bulk and display no obvious relation with the order–disorder transition in the bulk.

3.2.3. Sublattice occupancy. The occupancies of the gold and copper sublattices are respectively characterized by the fractions $p^{\beta}_{\mathrm{Au}}(z, T)$ and $p^{\alpha}_{\mathrm{Cu}}(z, T)$. These fractions are shown as functions of the temperature in figure 6. The results at the boundary, in the neighbouring mixed planes and in the bulk are again compared.

The case of the boundary plane and its first-neighbour mixed plane is particularly interesting. The fact that at $0.25\,T_c$, $p^{\beta}_{\mathrm{Au}}(z, T)$ is large and and $p^{\alpha}_{\mathrm{Cu}}(z, T)$ is small, results from the strong gold segregation effect. The fact that, at the same temperature, $p^{\beta}_{\mathrm{Au}}(z, T)$ is not equal to unity indicates that copper occupies some gold lattice sites and, in contrast to the case for the bulk, the gold sublattice is disordered. As the temperature increases, $p^{\beta}_{\mathrm{Au}}(z, T)$ decreases consistently with the decrease of segregation described above. At the same time $p^{\alpha}_{\mathrm{Cu}}(z, T)$ increases above 0.5. Two reasons may therefore be advanced. Either

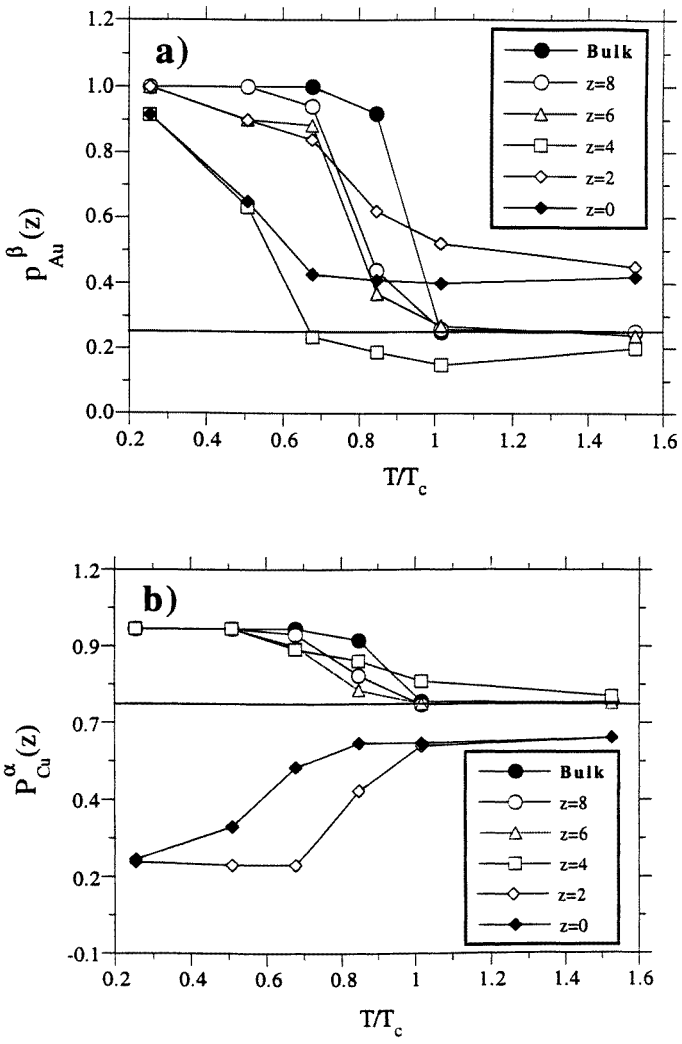

Figure 6. The occupancy fraction represented plane by plane as a function of temperature. Results for the bulk mixed planes are shown for comparison. (a) The fraction of occupancy of gold sites by gold atoms; and (b) the fraction of occupancy of copper sites by copper atoms. The grain boundary plane is at $z = 0$.

the increase is due to copper or it is due to the ordering of the copper superlattice with increasing temperature. The two phenomena may take place simultaneously. Above T_c, neither fraction is very temperature dependent any longer. In other words, either the orders in the two sublattices have opposite temperature dependence, or the segregation of one species is balanced by the depletion of the other, or both.

The situation in the plane at $z = 4$ is very peculiar. Like in the bulk, both sublattices are close to being perfectly ordered at low temperature. As the temperature increases however, only the gold sublattice becomes disordered. Whatever the strength of segregation is, the order may be measured by the ratio $R = p^{\beta}_{\mathrm{Au}}/C_{\mathrm{Au}}$. The gold sublattice is fully ordered when $R = 1/C_{\mathrm{Au}}$ and fully disordered when $R = 1$, irrespective of the value of C_{Au}.

A comparison between figures 5 and 6 shows that at $z = 0$, R is close to unity over the whole temperature range investigated, while at $z = 2$, it is about 1.1 for $T < T_c$ and 1 for $T > T_c$. At $z = 4$, a decrease from $R = 1.8$ at $0.25\,T_c$ to $R = 1.25$ at T_c is found and the present results indicate that this decrease proceeds still further, beyond T_c. Hence, the boundary plane is fully disordered at all temperatures, residual order is found in the next-neighbour mixed plane, and order is a smoothly decreasing function of temperature which proceeds above T_c. This is not specific to the actual grain boundary, as it has already been suggested on the basis of experimental observation of Cu_3Au surfaces [28].

The fact that around $0.8\,T_c$, $p^{\beta}_{\mathrm{Au}}(z, T)$ is about equal to the gold concentration reveals that most of the gold atoms present in this layer sit at gold sites.

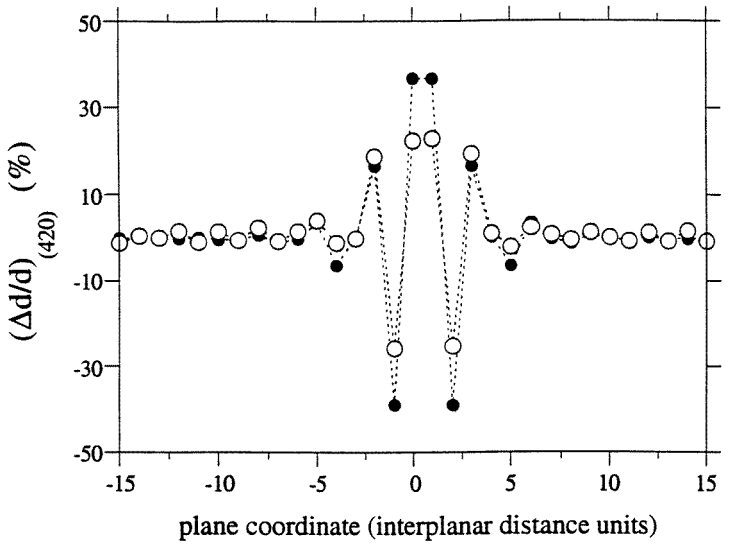

Figure 7. A comparison of relaxation profiles at 0 K (black circles) and 900 K (open circles).

At $z = 6$, the thermal evolutions of $p^{\beta}_{\mathrm{Au}}(z, T)$ and $p^{\alpha}_{\mathrm{Cu}}(z, T)$ are similar to the expectation for the bulk, although the gold sublattice disordering is faster than that of the copper one. We can thus distinguish between three regimes: one, in the bulk, which is related to the order–disorder phase transition; a second in the grain boundary plane which is fully disordered at all temperatures; and the third one, intermediate between the boundary and the bulk region, where the gold sublattice disorders, partially as a consequence of copper segregation.

At temperatures above T_c, there is no longer any thermal dependence of the order found close to the boundary and in the bulk, while it is still found in between.

3.2.4. Relaxation effects. Figure 7 shows the relaxation coefficient, plane by plane, around the boundary at 0 K and at $1.5\,T_c$. It is 37% at 0 K and 22% at $1.5\ T_c$.

The relaxation at the grain boundary is thus very large and remains large at temperatures well above T_c. In addition the oscillatory behaviour of $(\Delta d/d)_{(420)}$ around the grain boundary plane remains large at all temperatures investigated. This effect is thus better related to the atomic arrangement in the interface than to segregation of either copper or gold.

4. Discussion and conclusion

Among the many grain boundaries considered in [15], $\Sigma = 5$ (210) [001] of Cu_3Au was considered by spot, apparently using the same S_{51} configuration as in the present work and observed experimentally. This allowed us to cross check some of the results presented with ours, which is not often possible with computer simulation data. In the present work, we focus on the detailed thermal evolution of a grain boundary selected for its particularly large relaxation, segregation and disorder, rather than looking at common properties of several grain boundaries at selected temperatures as was done in [15] for different purposes.

The S_{51} configuration was identified by HREM; this is consistent with the fact that its computed excess energy is the lowest among the four variants considered.

In order to distinguish between chemical and structural effects, a comparison between occupancy probabilities and relative concentrations was necessary. In the case of the $\Sigma = 5$ (210) [001] boundary, the long-range order parameter (equation (9)) provides qualitatively correct predictions. The comparison allowed us to demonstrate that full disorder occurs in the grain boundary plane at all temperatures investigated, below and above T_c. More than ten per cent residual order is found in the next-neighbour mixed plane for $T > T_c$. In the same temperature range, a sharp transition between grain boundary and bulk ordering properties occurs between planes at $z = 4$ and $z = 6$, and the disordered zone does not expand continuously from the grain boundary to the bulk as the temperature increases. This contrasts with the results given in [15] in the case of a $\Sigma = 29$ boundary, thus showing that the strength of the coupling between the bulk and the boundary is dependent on the relative grain orientation. The temperature dependencies of the proper sublattice occupancy at the selvedge of the grain boundary are different.

While the correlation between disorder and segregation is found to be close to 1 over the whole temperature range below T_c, relaxation is only slightly sensitive to the segregation state in a range between $0.25\,T_c$ and $1.5\,T_c$, and it consequently plays no significant role in the thermal dependence of the segregation state of the grain boundary.

The most crucial parameter on which the present simulations are based is the potential. The potential used in the preceding section (model A) was designed in order to describe the cohesion of transition metals and their alloys, which are characterized by a partially filled d band. This is not the case for copper, and neither is it the case for gold, and, as a consequence, it is also not the case for copper–gold. The nature of the cohesion in noble metals is much more complex—in particular for elements as heavy as gold—and its full detail is accounted for in no cohesion model known to us. The same problem occurs for model B.

The use of these models is justified on an empirical basis, as they allow one to predict many experimentally observed properties of copper and gold. Both are based on equation (1) and they are thus quite similar. They do however differ in detail: in the description of the second moment of the electronic distribution in terms of a set of cubic splines in model A and in terms of Born–Mayer-like exponential functions in model B. The parameters of each were adjusted on the basis of measured elastic constants and some energetic properties of Cu_3Au. The questions which arise at this point are those of to what extent such an empirical adjustment of the potential parameters is valid for the prediction of further properties of Cu_3Au and to what extent the description presented in section 3 is sensitive to small changes in the potential model. The purpose of what follows is to address these questions. A subsequent question which naturally follows the former ones is that of to what extent the present study makes possible further improvement of the available cohesion models.

To consider the first question, let us focus on model B. In addition to the elastic

constants, (i) the lattice parameter, (ii) the mixing enthalpy of Cu_3Au, and (iii) the transition temperature for the order–disorder transition were used to adjust the model parameters. The latter parameter was however estimated on a rigid lattice [9]. In the present work, it is necessary to allow for relaxation in order to model the $\Sigma = 5$ (210) [001] boundary realistically, at the expense of the vibrational entropy inducing an important decrease of the estimated value of T_c in a perfect crystal. The same is found for the antisite energy.

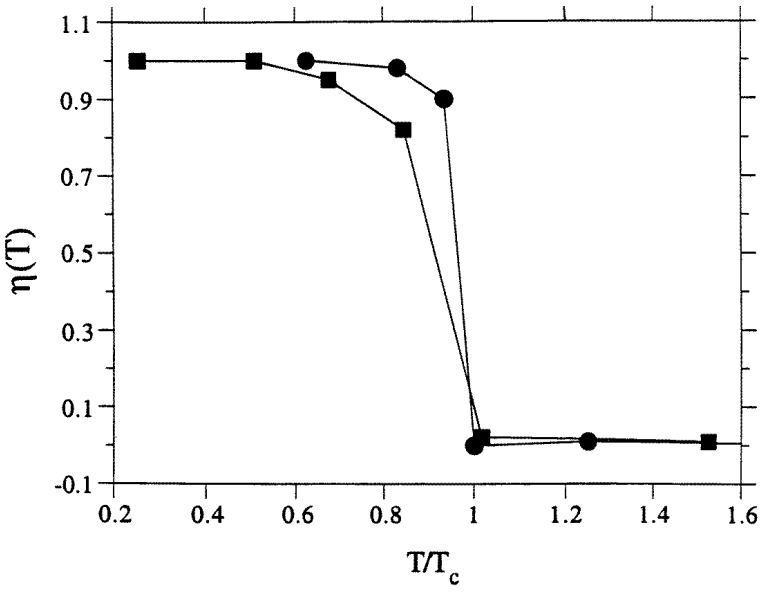

Figure 8. A comparison of the temperature dependence of the order parameter in a single crystal as obtained with the model potentials A (squares) and B (circles).

It was suggested [10] that T_c may reasonably be handled as a scaling factor in the description of the thermal properties of Cu_3Au. This implies that consistency should be found between somewhat different models provided that the same thermal parameter T/T_c is used for the description. Figure 8 shows the long-range order parameter as a function of T/T_c as predicted by models A and B for a perfect single crystal. It demonstrates a reasonable qualitative scaling. We adopt the scaling scheme in what follows, and its validity will be further discussed on the basis of a comparison between the results obtained with models A and B.

Although the predicted T_c-value is smaller with model B, the transition is sharper, which is more consistent with its experimentally observed first-order character. Since the discussion of the order of the transition is not the main purpose of this study, model A was used in the preceding section because it predicts an order–disorder temperature closer to the experimental value when relaxation is taken into account. Another reason, which is practical, is that it makes use of a smaller cut-off radius, with the consequence of faster computations. These reasons are of course not sufficient to prove the significance of the description in section 3 and we now address the second question of this section systematically. Many of the simulations presented in section 3, were repeated with model B for comparison, and this comparison is now presented in the same order as in section 3.

Examining the order parameter plane by plane, it was found with model A that the

thermal dependence of the order was completely different in the vicinity of the grain boundary to that in the bulk. This is confirmed by model B. Model A predicts that the vicinity extends up to $z = 8$ (figure 4). Model B predicts this vicinity to be much narrower. Even the first mixed plane neighbouring the grain boundary ($z = 2$) is significantly ordered at low temperature. Both models agree that η becomes temperature independent above T_c for all values of z. They also both agree in predicting full disorder in the grain boundary plane for temperatures ranging from $0.25\,T_c$ to $1.5\,T_c$.

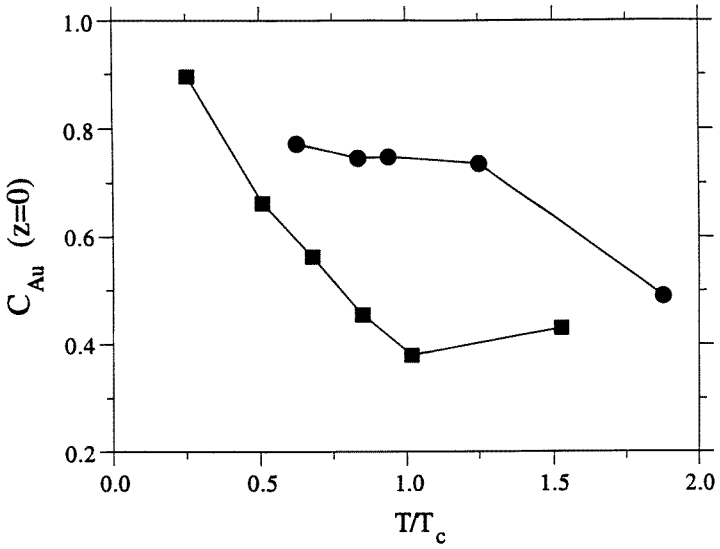

Figure 9. A comparison of the temperature dependence of the gold concentration in the boundary plane as obtained with the model potentials A (squares) and B (circles).

Examining the gold concentration plane by plane, it was found with model A that, like for η, its thermal dependence in the close vicinity of the boundary plane was different to that in the bulk. This is confirmed by model B. However, the thermal dependencies found with both models are in significant disagreement. This is illustrated in figure 9 where the results for the boundary plane ($z = 0$) are compared. A clear failure of the scaling assumption is found here. While model A predicts a decrease of the gold segregation up to T_c and concentrations below stoichiometric at T_c and above, model B predicts a strong gold segregation, almost independent of the temperature, up to well above T_c, followed by a tendency to reach the stoichiometric value at high temperatures ($T = 1.8\,T_c$).

Examining the sublattice occupancy fractions plane by plane, a monotonic decrease of p^{β}_{Au} with temperature was found, correlated with a monotonic increase of p^{α}_{Cu} in the boundary plane and its first-neighbour mixed plane. For more distant planes, the proper occupancy fraction dependence on temperature is influenced by the bulk. These observations are confirmed by model B for p^{β}_{Au} but not for p^{α}_{Cu}. Here again a significant difference is found. The increase of the copper fraction in its proper sublattice with increasing temperature is confirmed in the grain boundary plane, but not in its first-neighbour mixed plane, where p^{α}_{Cu} is predicted to be close to being temperature independent with model B, below as well as above T_c.

The occurrence of three distinct regimes at $z = 0$, close to the boundary plane, and in the bulk, is however, evident with both models.

Finally, the predicted interplanar relaxations are much the same for both models at all of the temperatures investigated.

It comes out of this comparison that the two models consistently describe many of the features investigated, which gives confidence in their applicability.

Some significant discrepancies are found however, which suggest an answer to the third question stated at the beginning of this section. The cohesive models underlying the present simulations were empirically adjusted, and the above-mentioned discrepancies suggest that atomic-scale observations of the $\Sigma = 5$ (210) [001] grain boundary may be useful in order to adjust them better. Indeed, high-resolution transmission electron microscopy allows an analysis plane by plane, just as performed in this simulation study. The relaxation plane by plane had already been studied quantitatively in the vicinity of an antiphase boundary in Cu_3Au and compared to the simulation with model B [27]. Good agreement was found. On the other hand, bicrystals with a $\Sigma = 5$ (210) [001] boundary are available, suggesting that a similar study could be performed of its vicinity. In addition, since contrast analysis combined with image processing now allows chemical composition studies, the different predictions of models A and B shown in figure 9 could be checked at least at low temperature. Further development of the high-resolution electron microscopy technique should make the observation of temperature dependencies a realistic prospect.

Acknowledgments

The authors are most grateful to V Pontikis for many stimulating discussions throughout the course of this work. It is also their pleasure to acknowledge discussions with all of the partners in the EEC contract SC1-CT91-0703 (TSTS) under which this work was achieved.

References

[1] See, e.g.,
Liu G T 1992 *Scr. Metall. Mater.* **27** 25
Lee T C, Robertson I M and Bernbaum H K 1992 *Acta Metall. Mater.* **40** 2569
Yoo M H, Sass S L, Fu C L Mills M J and George E P 1993 *Acta Metall. Mater.* **41** 987
[2] Kurmakov N, Zemczuzny S and Zasadelev M 1916 *J. Inst. Met.* **15** 305
[3] See, e.g.,
Antonopoulos J G, Schapink F M and Tichelaar F D 1990 *Phil. Mag. Lett.* **61** 195
Tichelaar F D, Schaping F W and Li X 1992 *Phil. Mag.* A **65** 913
Ricolleau C and Loiseau A 1993 *Mater. Sci. Forum* **126–128** 93
[4] Finel A 1992 *Ordering and Disordering in Alloys* ed A R Yavary (London: Elsevier) p 182
[5] Seah M P 1980 *J. Phys. F: Met. Phys.* **10** 1043
[6] Ducastelle F 1970 *J. Physique* **31** 1055
[7] Finnis M W and Sinclair J E 1984 *Phil. Mag.* A **50** 45
[8] Daw M S and Baskes M I 1983 *Phys. Rev. Lett.* **50** 1285
[9] Rey-Losada C, Hayoun M and Pontikis V 1993 *Mater. Res. Soc. Symp. Proc.* **291** 549
[10] Polatoglou H M and Bleris G 1994 *Interface Sci.* **2** 31
[11] Foiles S M 1985 *Phys. Rev.* B **32** 7685
[12] Udler D and Seidman D N 1995 *Interface Sci.* **3** 41
[13] Foiles S M and Seidman D M 1992 *Material Interfaces: Atomic Level Structure and Properties* ed D Wolf and S Yip (London: Chapman and Hall) p 497
[14] Seki A, Seidman D N, Oh Y and Foiles S M 1991 *Acta Metall. Mater.* **39** 3167
Udler D and Seidman D N 1992 *Phys. Status Solidi* b **172** 267; 1993 *Mater. Sci. Forum* **126–128** 165, 169; 1994 *Acta Metall. Mater.* **42** 1959
[15] Min Yan and Vitek V 1995 *Interface Sci.* **3** 17
[16] Ackland G J and Vitek V 1990 *Phys. Rev.* B **41** 10 324
[17] Ackland G J, Tichy G, Vitek V and Finnis M W 1987 *Phil. Mag.* A **56** 735

[18] Dumez C, Hayoun M, Rey-Losada C and Pontikis V 1994 *Interface Sci.* **2** 45
[19] Tichelaar F D 1990 *PhD Thesis* Delft University
[20] Farkas D and Yoo M H 1987 *Mater. Res. Soc. Symp. Proc.* **81** 99
[21] El Azzaoui M, Penisson J M and Pontikis V 1994 *Interface Sci.* **2** 79
[22] Bennet C H 1975 *Diffusion in Solids: Recent Developments* ed A S Nowick and J J Burton (New York: Academic) p 75
[23] Kroll D M and Gompper G 1987 *Phys. Rev.* B **36** 7078
[24] Chen S P, Voter A F and Srolovitz D J 1986 *Scr. Metall.* **20** 1389
[25] Polatoglou H M 1994 *Interface Sci.* **2** 67
[26] El Azzaoui M, Hou M and Pontikis V 1994 *Interface Sci.* **2** 57
[27] Potez L, El Azzaoui M, Loiseau A and Penisson J M, to be published
[28] Stuck A, Osterwalder J, Schlapbach L and Poon H C 1991 *Surf. Sci.* **251/252** 670